第 34 卷第 1 期
2018 年 1 月

无 机 化 学 学 报
CHINESE JOURNAL OF INORGANIC CHEMISTRY

Vol.34 No.1
63-72

表面化学侵蚀改性富锂层状正极材料 $Li[Li_{0.2}Mn_{0.54}Ni_{0.13}Co_{0.13}]O_2$

胡国荣 王伟刚 杜 柯* 彭忠东 曹雁冰
(中南大学冶金与环境学院,长沙 410083)

摘要：采用 3 种不同 pH 值的去离子水,NH_4NO_3 和 $H_2C_2O_4$ 溶液对富锂层状正极材料 $Li[Li_{0.2}Mn_{0.54}Ni_{0.13}Co_{0.13}]O_2$ 进行表面化学侵蚀改性,旨在改善其整体电化学性能。ICP 结果表明 pH 值对材料中 Li 的析出具有显著影响。X 射线衍射(XRD)表明表面化学侵蚀对材料的结构有影响。拉曼光谱(Raman spectroscopy)表明材料表面结构发生了变化。$H_2C_2O_4$ 溶液侵蚀过的样品的首次效率有了极大提高,但同时中值电压和循环性能显著恶化。NH_4NO_3 溶液侵蚀过的样品的首次效率从 63%提高到了 85%,1C 倍率下的放电比容量从 149 mAh·g^{-1} 提高到 194 mAh·g^{-1},同时保持了温和的中值电压变化曲线。通过高分辨透射电镜(HRTEM),X 射线光电子能谱(XPS)和电化学阻抗谱(EIS)对改性机理进行了研究。

关键词：正极材料；富锂层状；锂离子电池；表面改性
中图分类号：O646 **文献标识码**：A **文章编号**：1001-4861(2018)01-0063-10
DOI:10.11862/CJIC.2018.018

Surface Modification by Chemical Leaching of Over-Lithiuated Cathode Material $Li[Li_{0.2}Mn_{0.54}Ni_{0.13}Co_{0.13}]O_2$

HU Guo-Rong WANG Wei-Gang DU Ke* PENG Zhong-Dong CAO Yan-Bing
(*School of Metallurgy and Environment, Central South University, Changsha* 410083, *China*)

Abstract: With a purpose to improve the comprehensive electrochemical performance of over-lithiuated cathode material, surface modification was adopted using three solutions with specific pH value, including deionized water, NH_4NO_3 and $H_2C_2O_4$. The structure, morphology and electrochemical performance of the samples were extensively studied. ICP results show pH value has significant effect on the extraction of Li element in the materials. XRD demonstrates that the structure of the pretreated samples changed compared with the pristine sample. Raman Spectroscopy detects structural changes on the sample surface. The initial efficiency of $H_2C_2O_4$ treated sample is improved greatly but its mean voltage and cyclability is deteriorated simultaneously. The NH_4NO_3 treated sample shows the optimal comprehensive performance. Compared to the pristine sample, its initial coulombic efficiency is improved from 63% to 85% and capacity at 1C is enhanced from 149 to 194 mAh·g^{-1} while maintaining a mild mean voltage decay rate. The improvement mechanism has been investigated by high resolution transmission electron microscopy (HRTEM), X-ray Photoelectron Spectroscopy (XPS) and electrochemical impedance spectroscopy (EIS).

Keywords: cathode material; over-lithiuated; lithium ion battery; surface modification

收稿日期:2017-07-11。收修改稿日期:2017-10-23。
国家自然科学基金(No.51602352)资助项目。
*通信联系人。E-mail:duke22@csu.edu.cn

0 Introduction

Lithium ion battery has been considered as the most promising candidate for the EVs and rechargeable power station. As the key component in lithium ion battery, cathode material has been widely researched and greatly developed[1]. The explosive growth of electric vehicles calls for a suitable cathode material with high enough energy density[2]. Among the cathode materials used at present, over-lithiuated cathode material with a general formula of $Li[M_{1-x}Li]O_2$ (M=Mn, Ni, Co) has evoked great interest due to its high capacity and good thermal stability. It can reach a practical capacity of 250 mAh $\cdot g^{-1}$ or more when charged above 4.5 V. Moreover, due to the high content of Mn, it possesses the advantages of cost-effectiveness, environment benignity, and operation safety[3-8]. When initially charged above 4.3 V, cells with over-lithiuated cathode material exhibit a unique voltage profile. This profile can be generally divided into two regions: a sloping region to 4.4 V and a plateau between 4.4 and 4.7 V. When charged to 4.4 V, lithium is extracted from the $LiMO_2$ component. The Li_2MnO_3 domains are electro-chemically inactive under 4.4 V; at higher potentials lithium is removed from the structure with concomitant oxidation of the oxygen ions, while the manganese ions maintain their tetravalent oxidation state. Simplistically, this process can be represented by the electrochemical removal of lithium and oxygen from the Li_2MnO_3 structure, the net loss being "Li_2O", which results in a significant first-cycle capacity loss. As a result, the following bottlenecks are urgently required to be settled before put into large-scale application: (1) low initial coulombic efficiency and large irreversible capacity(C_{Ir})[5,8]; (2) poor rate capability and its capacity is far less than 200 mAh $\cdot g^{-1}$ at 1C[9-12]; (3) poor cyclability due to decomposition of electrolyte under the high cut-off voltage[8-9]; (4) voltage decaying arising from the structure transformation and hence resulting decrease of energy density[13-15].

Doping into structure and surface modification are the main improving methods for all kinds of cathode materials. In view of its specific composition, surface treatment is proved to be an effective way to improve the comprehensive performance of over-lithiuated cathode materials. Thackery et al.[16] stated acid treatment could improve the initial coulombic efficiency. Simultaneously, a more stable spinel-like structure formed on the surface after the reaction between the acid and surface material and supplies additional channel for the intercalation and deintercalation of Li^+ ions. Kang et al.[17] treated $0.3Li[Li_{1/3}Mn_{2/3}]O_2 \cdot 0.7Li[Ni_{1/2}Mn_{1/2}]O_2$ with HNO_3 and the initial coulombic efficiency was enhanced to 82%. But the high acidity damaged the surface structure, which led to the deterioration of cyclability and rate capability. Denis et al.[18] treated $Li[Li_{0.2}Mn_{0.54}N_{i0.13}Co_{0.13}]O_2$ with $(NH_4)_2SO_4$ solution and confirmed the existence of a lithium-poor spinel structure on the surface.

To take a systematic study on the effect of surface modification on initial coulombic efficiency, rate and cycle capability and voltage decaying, obtain the optimal improving method and further understand its mechanism, we adopted three solutions with specific pH values. $Li[Li_{0.2}Mn_{0.54}Ni_{0.13}Co_{0.13}]O_2$ was fabricated by conventional co-precipitation method as pristine sample and treated with deionized water, NH_4NO_3 and $H_2C_2O_4$ solution, whose pH value is about 6.8, 3.9 and 1.3, respectively. The four samples are characterized by Inductively coupled plasma (ICP), X-ray diffraction (XRD), Scanning electron microscope (SEM), high-resolution transmission electron microscopy (HRTEM), Raman spectroscopy, X-ray photoelectron spectroscopy (XPS), charge-discharge measurements and electrochemical impedance spectroscopy (EIS) to develop a comprehensive and in-depth understanding of the functions of the treatment solutions.

1 Experimental

The precursors of the pristine $Li[Li_{0.2}Mn_{0.54}Ni_{0.13}Co_{0.13}]O_2$ material was synthesized via a carbonate co-precipitation method using $NiSO_4 \cdot 6H_2O$ (AR, ≥98.5%), $CoSO_4 \cdot 7H_2O$ (AR, ≥98.5%), Na_2CO_3 (AR, ≥99.8%) and $MnSO_4 \cdot H_2O$ (AR, ≥99%) as raw materials. The particle size was controlled by the dropping speed and reaction time. Dropping speed

was 0.8~1 mL·min^{-1} and reaction time was 10 h under continuous stirring. The pH value was maintained was at 8~8.5 by controlling the dropping speed of Na_2CO_3 and $NH_3 \cdot H_2O$. After filtration, rinsing and drying, precursors can be obtained. A mixture of precursor and Li_2CO_3 with $n_{Li}:n_M=1.5$ is calcined to produce Li $[Li_{0.2}Mn_{0.54}N\ i_{0.13}Co_{0.13}]O_2$ cathode material at 900 ℃ for 10 h.

Three pieces of 2 g pristine sample were added into 200 mL treatment solutions including deionized water, NH_4NO_3 and $H_2C_2O_4$, whose pH values were maintained around 6.8, 3.9 and 1.3 respectively. The mixed solutions were treated in 50 ℃ supersonic water bath for 10 min then washed and filtered for several times. Then the samples were dried in an 120 ℃ oven and calcined under 500 ℃ for 3 h. For the sake of simplicity, the pristine sample and samples treated with deionized water, NH_4NO_3 and $H_2C_2O_4$ solution were named as Sample **A**, **B**, **C** and **D** respectively.

Inductive coupled plasma technique (ICP-AES spectrometer Ultima-2 from Jobin Yvon Horiba) was used for the elemental analysis of samples. The crystal structure of all samples were characterized by using X-ray diffraction (Riguku θ/θ diffractometer with Cu $K\alpha$ radiation, λ=0.154 05 nm). XRD data were obtained in 2θ range of 10°~80°, with a scan speed of 2°·min^{-1}. The morphological features and particle sizes were observed by scanning electron microscope equipped with EDXS energy disperse X-ray spectrometer (SEM, Hitachi X-650) and high-resolution transmission electron microscopy (HRTEM, FEI TecnaiF20). Raman spectroscopy was carried out on a micro-Raman spectrometer from Renishaw (UK) equipped with a 514 nm laser, a CCD camera, and an optical Leica microscope. A 50x objective lens was used to focus the incident beam and an 1 800 lines per mm grating was used. For each sample, the spectra were recorded from three to five locations. XPS data were collected at room temperature with a Kratos Analytical Spectrometer and monochromatic Al $K\alpha$ (1 486.6 eV) X-ray source to assess the chemical state of elements on the treated surface layers.

The charge-discharge tests were carried out by assembling 2025-type coin cells with a lithium metal anode, working cathode and Celgard 2400 microporous membrane. The working cathode was fabricated by blending active material, acetylene black and PVDF binder (8∶1∶1). A $LiPF_6$ solution of 1 mol·L^{-1}, dissolved in ethylene carbonate (EC)/dimethyl carbonate (DMC) (1∶1, *V*/*V*), was employed as the electrolyte. The charge-discharge tests were carried out on a Land electrochemical test instrument. The cells were charged and discharged at various rates and their initial coulombic efficiency, mean voltage, rate capability and capacity retention were recorded. Electrochemical impedance spectroscopy (EIS) of the cells was conducted on an electrochemical workstation (CH Instrument). EIS experiment was carried out after the cells were assembled and rested for several minutes. The frequency range was 0.001 Hz~100 kHz at alternating current signal amplitude of 10 mV.

2 Results and discussion

2.1 Material characterization

The contents of Li, Mn, Ni and Co elements in the filtrate from washing the treated samples are listed in Table 1. It can be seen that the filtrate from Sample **B** contains 3.26% (*w*/*w*) Li and a trace of transition metal elements. The elements in the filtrate from Sample **C** are mainly composed of Li which reaches up to 10.45% (*w*/*w*). The Li content in the filtrate from Sample D is as high as 15.28%(*w*/*w*) as a result of the high acidity of $H_2C_2O_4$. It can be also concluded from the table that the extraction of transition metal elements increases with the increasing of the acidity of treatment solutions. According to the loss of elements, the formula of the treated samples can be rewritten as $Li_{1.1471}[Mn_{0.54}Ni_{0.13}Co_{0.13}]O_2$ (Sample **B**), $Li_{1.062}[Mn_{0.54}Ni_{0.13}Co_{0.13}]O_2$ (Sample **C**) and $Li_{1.0045}[Mn_{0.5025}Ni_{0.1211}Co_{0.1271}]O_2$ (Sample **D**).

Fig.1 displays the XRD patterns of all the samples. By comparing the patterns of the treated sample with the pristine one, it can be confirmed that all the XRD patterns show a clear split between the (006)/(102) and (108)/(110) peaks and no other impurity

Table 1 Weight percentage of elements dissolved out during treatment process

Sample	w_{Li} / %	w_{Ni} / %	w_{Co} / %	w_{Mn} / %
Sample **B**	3.26	0.005 7	0.005 7	0.002 8
Sample **C**	10.45	0.010 5	0.012 6	0.008 9
Sample **D**	15.28	0.071 3	0.080 2	0.067 5

peaks, which means that treatment haven′t changed the structure of the pristine sample significantly and all the samples have a well hexagonal structure[6,11,19]. The low intensity peaks around 21°~25° correspond to the superlattice peaks (PDF No.000-73-0152) caused by ordered arrangement of the ions when lithium enters the transition metal layer[8-9,20]. From partial enlargement of Fig.1 it can be found that this peak is weakened slightly after treatment. It can be assumed that the lithium amount in transition metal layer decreases after surface treatment, which evidences that the leached lithium element originates from the transition metal layer partially.

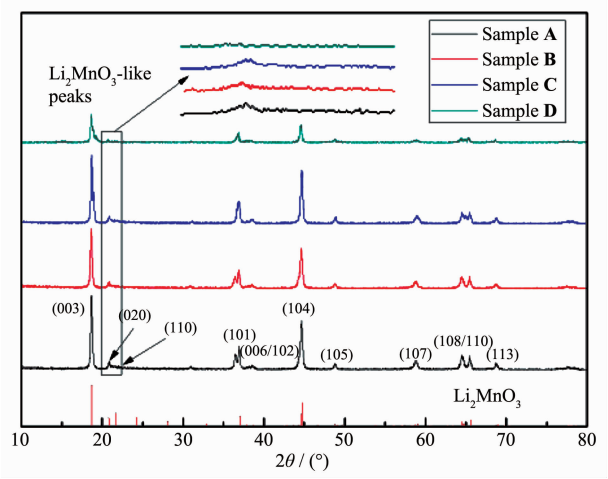

Fig.1 XRD patterns of $Li[Li_{0.2}Mn_{0.54}Ni_{0.13}Co_{0.13}]O_2$ samples

Unit cell parameters and intensity ratio of $I_{(003)}/I_{(104)}$ of all the four samples are obtained through Jade software and summarized in Table 2. Compared with Sample **A**, the lattice constant a of Sample **B**, **C** and **D** decreases, and c increases, which leads to the increasing of c/a value. It proves the solution treatment affects the bulk structure of the pristine material[19]. Lattice constant c could also characterize the interlayer spacing of MO_2 layer. The greater c value is, the greater is the interlayer spacing and also the diffusion channel for Li^+ ions in the layer structure. The c/a values of all the four samples are greater than 4.899, which indicates they have an ideal cubic close packed and well layered structure. For the layered structure materials such as $LiCoO_2$, c value increases with the deintercalation of Li^+ ions[1]. Hence, the increasing of c value of the treated samples proves that the leached Li element originates from the Li layer partially[21]. Noteworthy, the intensity ratio of $I_{(003)}/I_{(104)}$ also increases after solution treatment. Chung-Hsin et al.[22] stated that intensity ratio of $I_{(003)}/I_{(104)}$ can be used to determine the cation distribution in the lattice and a value lower than 1.2 indicated a high degree of cation mixing, primarily due to the occupancy of other ions in the lithium region, and the higher the ratio was, the lower the level of cation mixing was and the more beneficial to the lithium-ion transfer. As shown in Table 2, the intensity ratio of $I_{(003)}/I_{(104)}$ of all samples are greater than 1.5, which indicates a low level of cation mixing and a well layered structure of the materials[21]. The high intensity ratio of $I_{(003)}/I_{(104)}$ of the pristine sample is mainly determined by its composition and synthesis route. The intensity ratio of $I_{(003)}/I_{(104)}$ is generarlly inversely proportional to the nickel content in the material. Unlike the commercialized layered ternary materials, over-lithiuated oxide is rich in manganese

Table 2 Lattice parameters of $Li[Li_{0.2}Mn_{0.54}Ni_{0.13}Co_{0.13}]O_2$ samples

Sample	a / nm	c / nm	c / a	$I_{(003)}$ / $I_{(104)}$
Sample **A**	0.285 26	1.422 13	4.985 4	1.582 7
Sample **B**	0.285 15	1.423 17	4.990 9	1.684 6
Sample **C**	0.284 72	1.425 34	5.006 1	2.017 1
Sample **D**	0.284 58	1.425 53	5.009 2	1.873 2

and much lower in nickel, so it has a low degree of cation mixing and possesses a high intensity ratio of $I_{(003)}/I_{(104)}$.

SEM images of four samples are shown in Fig.2. It is obvious that the particles of pristine sample agglomerate and the particle size is estimated to be about 0.5 μm. Deionized water almost has no effect on its morphology. However, compared with the pristine sample, Sample **C** and **D** have more even distribution of grain size and the particles become smaller. This may be caused by the reaction between the surface and the treatment solutions.

Fig.3 shows HRTEM images of Sample **A** and **C**. Sample **A** has clear lattice fringes which prove a high degree of crystallinity of the pristine sample. It can be clearly detected that an amorphous layer which can be attributed to the reaction between the pristine sample surface and pretreatment solution spreads over the bulk structure of Sample **C**.

Raman spectroscopy is valuable to study the

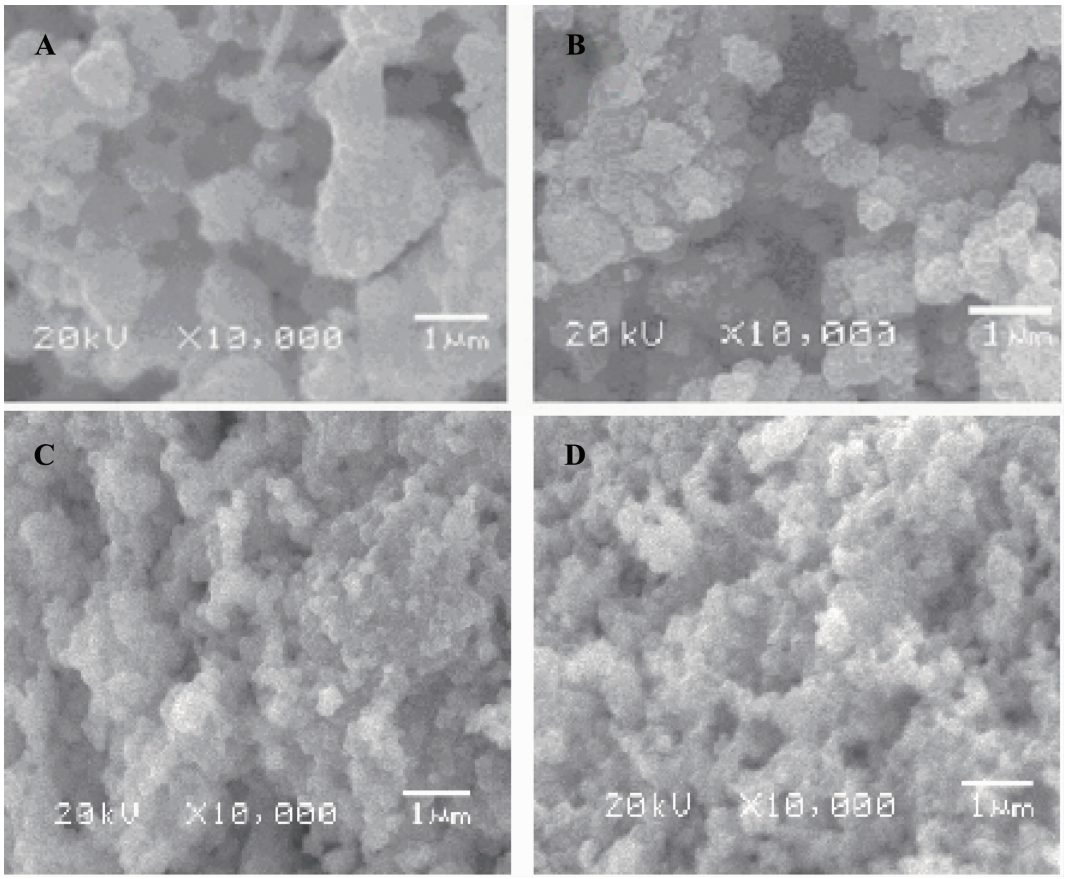

Fig.2　SEM images of $Li[Li_{0.2}Mn_{0.54}Ni_{0.13}Co_{0.13}]O_2$ samples

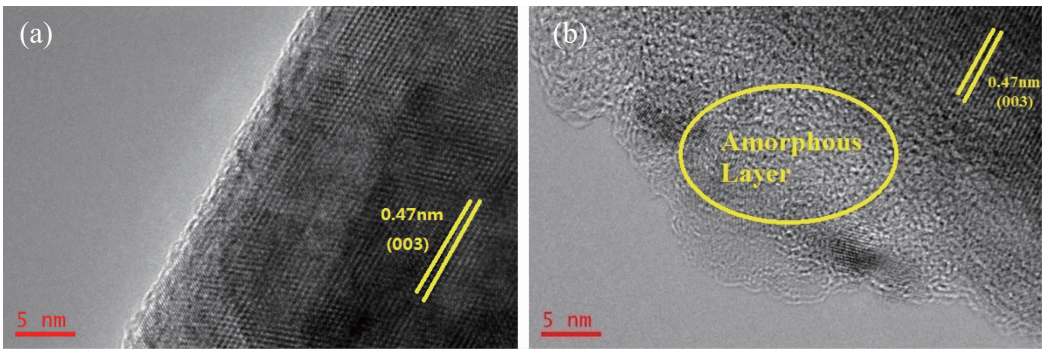

Fig.3　HRTEM images of Sample **A** (a) and **C** (b)

surface evolution of materials. Fig.4 compares the Raman spectra of all the four samples. All the three characteristic Raman bands of over-lithiuated are found in the spectra of Sample **A** and **B**. The Raman band at 422 cm^{-1}, which disappears in Sample **C** and **D**, is assigned to the monoclinic Li_2MnO_3 phase[18,23]. This proves the NH_4NO_3 and $H_2C_2O_4$ solutions can react with the Li_2MnO_3 component in $Li[Li_{0.2}Mn_{0.54}Ni_{0.13}Co_{0.13}]O_2$. The other two significant Raman peaks near 475 and 595 cm^{-1} in the spectra of Sample **A** and **B** belong to the bending E_g and stretching A_{1g} modes, respectively, which are blue shifted to higher values as to Sample **C** and **D**. It is reported that a pronounced blue shift of Raman bands is always observed upon cycling of these Li and Mn-rich cathode materials[23-25].

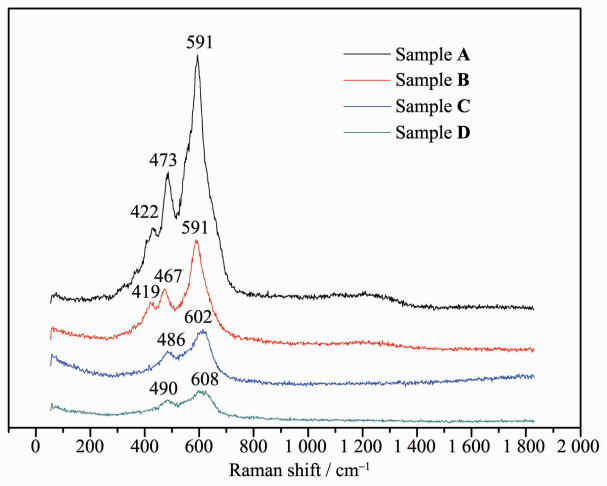

Fig.4 Raman spectra of $Li[Li_{0.2}Mn_{0.54}Ni_{0.13}Co_{0.13}]O_2$ samples

The oxidation states of the metal ions in the samples were determined by XPS. Fig.5 indicates the full spectrum and 2*p* spectrum of each transition metal split into two spin-orbit coupling components, $2p_{3/2}$ and $2p_{1/2}$. The energy separation between the two

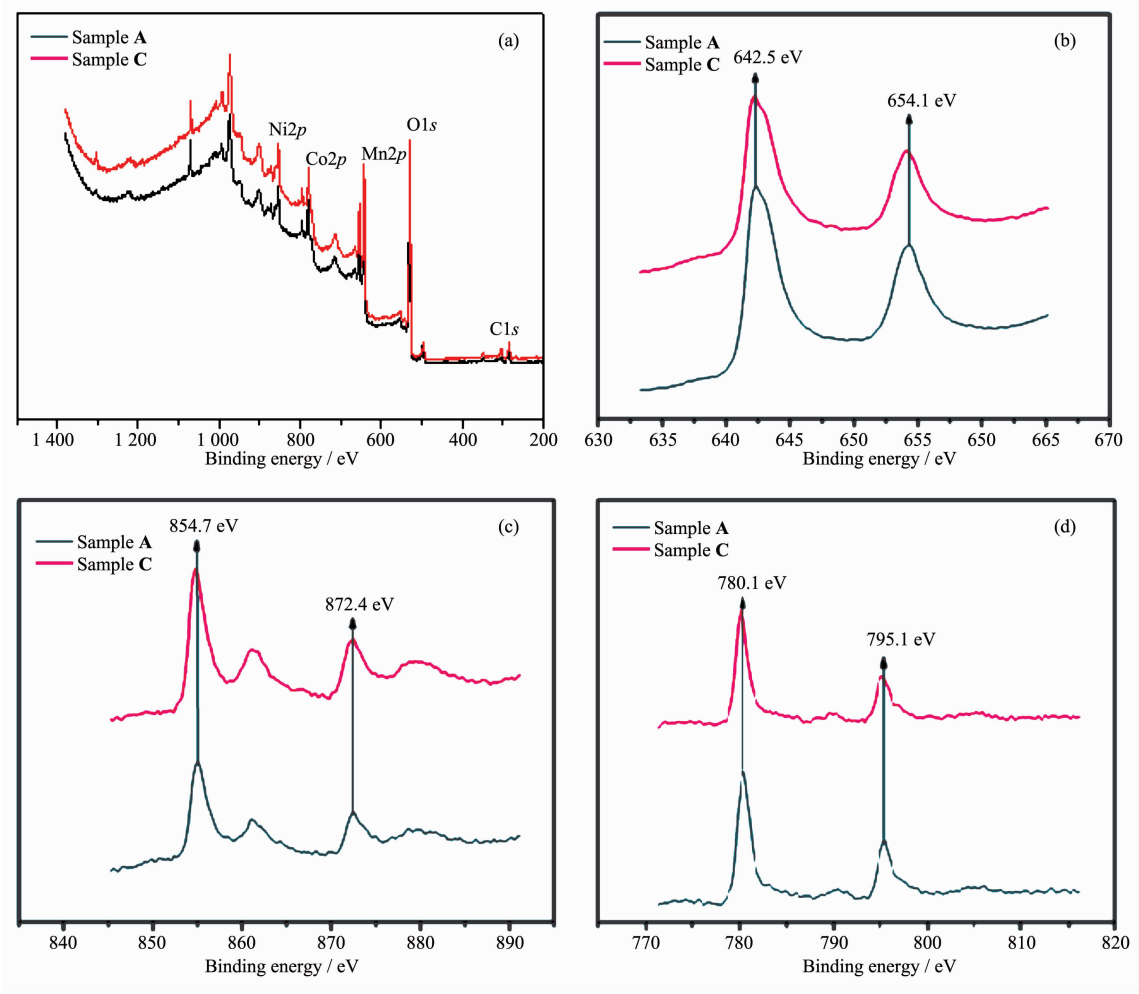

Fig.5 XPS spectra of Sample A and C: (a) full spectra, (b) Mn2*p*, (c) Ni2*p* and (d) Co2*p*

peaks is related to the mean oxidation state[26]. The full spectra in Fig.5(a) evidence Sample **A** and **C** contain Ni, Co, Mn, O and C elements. As shown in Fig.5(b), the Co2*p* spectra of both samples have two sharp peaks at 780.1 and 795.1 eV, which corresponds to $Co2p_{3/2}$ and $Co2p_{1/2}$ respectively. The binding energy gap is about 15 eV, confirming the existence of Co^{3+}[26-28]. Fig.5(c) displays the Ni2*p* spectra of the tested samples, in which two sharp peaks at 854.7 and 872.4 eV corresponding to $Ni2p_{3/2}$ and $Ni2p_{1/2}$ respectively can be seen. The binding energy gap is about 17.7 eV, confirming the existence of Ni^{2+}[28-29]. In Fig.5(d) the Mn2*p* spectra show two sharp peaks at 642.5 and 654.1 eV, corresponding to $Mn2p_{3/2}$ and $Mn2p_{1/2}$. The binding energy gap is about 11.5 eV, confirming the existence of Mn^{4+}[30-31]. The results prove that the Co, Ni and Mn elements on the surface exist in the form of Co^{3+}, Ni^{2+} and Mn^{4+} respectively and solution treatment has no effect on their valences.

2.2 Electrochemical properties

Fig.6 shows the initial charge-discharge curves of four samples between 2.0 and 4.8 V at 0.1C. As shown in Fig.6, the initial irreversible capacity (C_{Ir}) of the treated samples decreases compared to the pristine sample, among which the C_{Ir} of Sample B decreases slightly from 140 to 127 mAh·g^{-1} and the C_{Ir} of Sample **C** and **D** decrease prominently to 44.5 and 37.7 mAh·g^{-1}, respectively. Correspondingly, the efficiency was also enhanced from 63% to 65%, 85% and 86% respectively. Regarding the initial charge process of lithium-manganese-rich layered oxides, it is generally accepted that the whole process can be divided into two steps: Firstly, from the initial voltage to around 4.4 V, Li^+ ions deintercalate from the $LiMO_2$ component, which is the same as that of the conventional layered oxides, then it is followed that Li^+ and O^{2-} deintercalate from the LiM_2O_3 component above 4.4 V in the form of Li_2O[5,15-18]. Dividing the initial charge curve into two sections according to the fore-mentioned mechanism and comparing the capacity of each section of all the samples, it can be found the treatment of solutions has effect on the capacities of both sections and this proves that Li leached from the pristine sample originate from both the Li layer and transition metal layer, which is in well accordance with the XRD analysis results. Meanwhile, from Table 3 it is evident that the effect on the Li_2MnO_3 section is more significant, which is the key factor of the effect on initial efficiency. Denis et al.[18] proved that $(NH_4)_2SO_4$ solution could affect the Li_2MnO_3 component notably. Interestingly, the discharge capacity of all the samples almost show no difference, but the discharge curves of Sample C and D both show an additional curve marked by arrow in Fig.3, which can be detected in most Mn compounds[3,5-10]. This also proves that acid solution can react with the pristine material and form a new structure related to Mn elements. Based on the XPS analysis results, Denis et al.[18] confirmed this new structure is not spinel structure such as $LiMn_2O_4$. Kang et al.[17] confirmed the existence of H^+-ion exchanged and Li_2O/H_2O-deficient Li_2MO_3 product after reaction between the pristine material and HNO_3, which provides evidence for the argument on the composition of over-lithiuated oxide. The analysis on the capacity variation during the

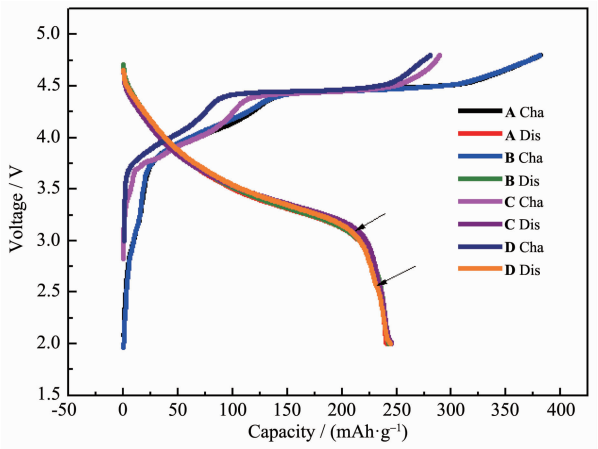

Fig.6　Initial charge-discharge curves of $Li[Li_{0.2}Mn_{0.54}Co_{0.13}Ni_{0.13}]O_2$ samples (0.1C)

Table 3　Charge capacity of $Li[Li_{0.2}Mn_{0.54}Ni_{0.13}Co_{0.13}]O_2$ samples in each section

Sample	C_{LiMO_2} / (mAh·g^{-1})	$C_{Li_2MnO_3}$ / (mAh·g^{-1})
Sample **A**	117.5	264
Sample **B**	112.4	256.4
Sample **C**	103.6	185.7
Sample **D**	102.8	179

initial cycle of all the samples as shown in Fig.6 is also in accordance with the statement of Kang et al.

Fig.7 depicts the rate performance of $Li[Li_{0.2}Mn_{0.54}Ni_{0.13}Co_{0.13}]O_2$ samples. It can be intuitively concluded that compared with Sample **A**, the capacity of Sample **B** at all rates increases little and the rate performance of Sample D at 0.1C, 0.2C and 0.5C improve greatly, but deteriorates at 1C with a capacity of 127 $mAh\cdot g^{-1}$, which may be due to the structure transformation after high acidity treatment. Kang et al.[17] stated when Li_2MnO_3 component was overactivated, too much Li_2O was removed from the parent structure, hence deteriorating the rate performance and cyclability. Sample **C** shows the optimal rate performance especially at high rate (1C) and the capacity at 1C reaches 194 $mAh\cdot g^{-1}$ which is much better than 149 $mAh\cdot g^{-1}$ of the pristine sample.

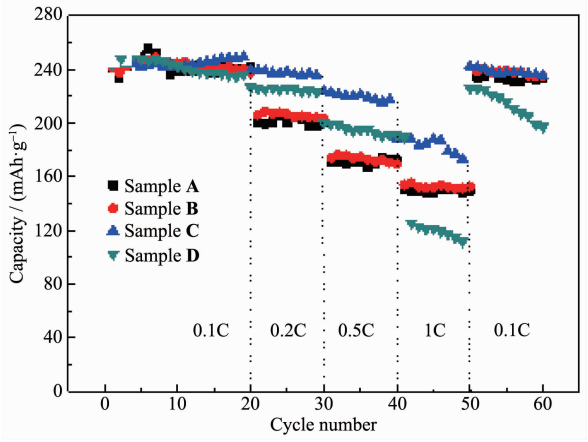

Fig.7 Rate capability of $Li[Li_{0.2}Mn_{0.54}Ni_{0.13}Co_{0.13}]O_2$ samples

From the discharge data of 20 cycles at 0.1C, it can be stated that Sample **A** reaches its peak at the 7th cycle and fades gradually, Sample **B** shows a similar tendency as Sample **A**, and Sample **D** shows the highest capacity at the initial cycle and fades in the subsequent cycles. Sample **C** shows an excellent cycle performance and has no decay after 20 cycles, which proves the NH_4NO_3 solution treatment is beneficial to the cycle performance of the pristine material. After 50 cycles at various rates, when back to 0.1C rate, all the samples except Sample **D** show a good capacity retention rate, which proves the layer structure are not damaged after the cycles even at high rate (1C), but over high acidity may damage the layer structure.

Moreover, it is worth noting that the capacity of the pristine sample keeps increasing for the first seven cycles. This activation process is considered to be related to the rearrangement of cations and orderly arrangement of transition metal ions in the stacking of materials[32]. In our previous study we treated $Li[Li_{0.2}Ni_{0.2}Mn_{0.6}]O_2$ with acids and decreased the activation cycle number from 17 to 5[33]. As seen from Fig. 5, Sample C and D almost need no activation cycle, which indicates the material has been activated and the cations has been rearranged in advance during the treatment process.

Fig.8 shows the tendency of mean voltage of all the four samples. Due to the structure transformation during the charge-discharge cycles, lithium-manganese-rich layered oxide suffers from voltage decay, which could affect the energy density in turn. In accordance with the results of Thackery et al.[5], the mean voltage of Sample **D** decreases sharply during the cycles, especially at high rate. The mean voltages of Sample **B** and **C** decay gradually, which is similar to that of Sample **A**. It is generally accepted that this phenomenon results from the new Mn-containing structure which generally has low voltage plateau than the pristine material[5,16]. Here it is worth noting that when back to 0.1C rate, the mean voltage cannot return to the previous value, which confirms the transformation

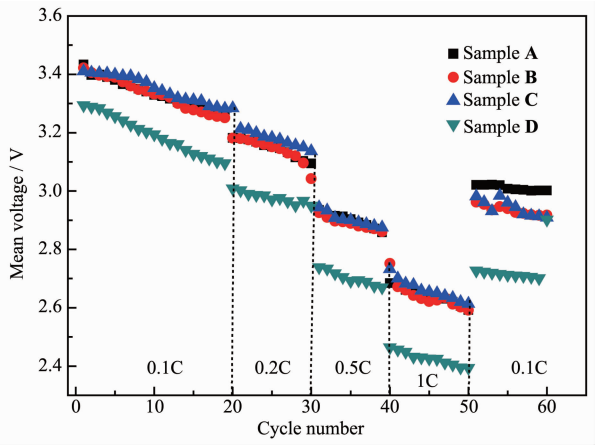

Fig.8 Mean voltage of $Li[Li_{0.2}Mn_{0.54}Ni_{0.13}Co_{0.13}]O_2$ samples corresponding to the charge-discharge cycles in Fig.6

of structure is irreversible.

EIS is conducted to investigate the electrochemical behaviors during the charge/discharge process. Fig.9 presents the EIS spectra for Sample **A**, **B**, **C** and **D** in half Li-cells. All cells were fresh and with an open circuit voltage (OCV) of ~2.9 V. The curves of samples exhibit a semicircle in the high-to-medium frequency region and a beeline in the low-frequency range, which represent charge-transfer resistance at the electrode/electrolyte interface and the diffusion resistance of lithium ions in the bulk electrode materials, respectively[11]. According to the Nyquist plots of the four samples, the apparent shrinkage of the semicircle in the sequence from Sample **A** to **B** till **C** unambiguously indicates the lowest charge transfer and surface film resistance of Sample **C**. The corresponding equivalent circuit model (Fig.9, inset) is composed of a system resistance (R_s), a constant phase element (CPE), a charge-transfer resistance (R_{ct}), and a Warburg impedance (Z_w)[34-35]. The calculated system resistances (R_s) are 2.57, 2.95, 2.66 and 2.48 Ω for Sample **A**, **B**, **C** and **D**, while the surface charge transfer resistance (R_{ct}) are 248, 130.6, 113 and 212.4 Ω, respectively. The result shows that Sample C has a much lower R_{ct} than the other three samples. This may result from the amorphous layer generated on the pristine sample surface after reaction with NH_4NO_3. The layer replaces the original interface and supplies a better electron diffusion channel through which the electron diffuses acceleratedly. The results are in well accordance with the rate capability of all the four samples.

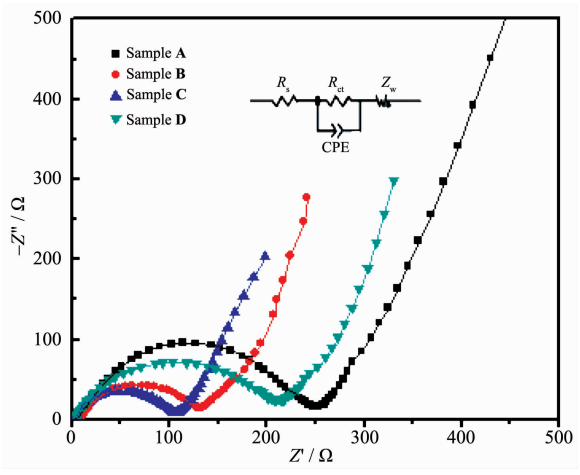

Fig.9　Nyquist plots of $Li[Li_{0.2}Mn_{0.54}Ni_{0.13}Co_{0.13}]O_2$ samples

3　Conclusions

Deionzied water, NH_4NO_3 and $H_2C_2O_4$ solutions were adopted to treat the surface of Li $[Li_{0.2}Mn_{0.54}Ni_{0.13}Co_{0.13}]O_2$. Surface treatment can affect the bulk structure of the pristine sample. The particle size became smaller after surface treatment as shown in SEM images. TEM confirms the formation of a new crystalline phase. XPS analysis proves no valence state change of the transition meal ions on the surface. The sample treated with NH_4NO_3 possesses the optimal comprehensive electrochemical performance. Its initial coulombic efficiency is enhanced to 85% and discharge capacity at 1C reaches 184 mAh·g^{-1}, comparing to 63% and 149 mAh·g^{-1} of pristine sample. EIS results show that surface treatment decreases the charge-transfer resistance and enhances the reaction kinetics, which is considered to be the major factor for better rate performance. The decaying of mean voltage during cycles needs to be further studied.

References:

[1] Honkura K, Horibab T. *J. Power Sources*, **2014**,**264**:140-146
[2] Xu K, Jie Z F, Li R H, et al. *Electrochim. Acta*, **2012**,**60**:130-133
[3] Gnanaraj J S, Pol V G, Gedanken A, et al. *Electrochem. Commun.*, **2003**,**5**(11):940-945
[4] Konarova M, Taniguchi I. *J. Power Sources*, **2010**,**195**(11):3661-3667
[5] Thackeray M M, Kang S H, Johnson C S, et al. *J. Mater. Chem.*, **2007**,**17**:3112-3125
[6] Chen H, He Z J, Huang Z M, et al. *Ceram. Int.*, **2017**,**43**(12):8616-8624
[7] Yu C, Li G, Guan X, et al. *Chem. Phys.*, **2012**,**14**:12368-12377
[8] Ohzuku T, Nagayama M, Tsuji K, et al. *J. Mater. Chem.*, **2011**,**21**:10179-10188
[9] Yu H J, Wang Y R, Asakura D, et al. *RSC Adv.*, **2012**,**2**:8797-8807
[10]Yu H J, Zhou H S. *J. Phys. Chem. Lett.*, **2013**,**4**:1268-1280
[11]Wang M, Luo M, Chen Y B, et al. *J. Alloys Compd.*, **2017**,

696:891-899

[12]Zhang H Z, Qiao Q Q, Li G R, et al. *J. Mater. Chem.*, **2012**, **22**:13104-13109

[13]Gu M, Belharouak I, Zheng J M, et al. *ACS Nano*, **2013**,**7**: 760-767

[14]Yu S H, Yoon T, Mun J Y, et al. *J. Mater. Chem. A*, **2013**, **1**:2833-2839

[15]Croy J R, Kim D H, Balasubramanian M, et al. *J. Electrochem. Soc.*, **2012**,**159**(6):A781-A790

[16]Johnson C S, Kim J S, Lefief C, et al. *Electrochem. Commun.*, **2004**,**6**:1085-1091

[17]Kang S H, Johnson C S, Vaughey J T. *J. Electrochem. Soc.*, **2006**,**153**(6):A1186-A1192

[18]Yu Denis Y W, Katsunori Y, Hiroshi N. *J. Electrochem. Soc.*, **2010**,**157**(11):A1177-A1182

[19]Gao Y, Yakovleva M V, Ebner W B. *Electrochem. Solid-State Lett.*, **1998**,**1**(3):117-119

[20]Park Y J, Hong Y S, Wu X, et al. *J. Power Sources*, **2004**, **129**:288-295

[21]Li J B, Xu Y L, Li X F, et al. *Appl. Surf. Sci.*, **2013**,**285** (11):235-240

[22]Lu C H, Wang H C. *J. Electrochem. Soc.*, **2005**,**152**(6):C341 -C347

[23]Nayak P K, Grinblat J, Levi M, et al. *Electrochim. Acta*, **2014**,**137**:546-556

[24]Amalraj F, Talianker M, Markovsky B, et al. *J. Electrochem. Soc.*, **2013**,**160**(2):A324-A337

[25]Nayak P K, Grinblat J, Levi M, et al. *J. Electrochem. Soc.*, **2014**,**161**:A1534-A1547

[26]Min J W, Gim J, Song J, et al. *Electrochim. Acta*, **2013**,**100**: 10-17

[27]Daheron L, Dedryvere R, Martinez H, et al. *Chem. Mater.*, **2008**,**20**:583-590

[28]Chang Z R, Chen Z J, Wu F, et al. *Electrochim. Acta*, **2008**, **53**:5927-5933

[29]Zhao Y, E Y F, Fan L Z, et al. *Electrochim. Acta*, **2007**,**52**: 5873-5878

[30]Jafta C J, Ozoemena K I, Mathe M K, et al. *Electrochim. Acta*, **2012**,**85**:411-422

[31]Park J S, Roh K C, Lee J W, et al. *J. Power Sources*, **2013**, **230**:138-142

[32]Armstrong A R, Holzapfel M, Novák P, et al. *J. Am. Chem. Soc.*, **2006**,**128**(26):8694

[33]DU Ke(杜柯), HUANG Xia(黄霞), YANG Fei(杨菲), et al. *Chinese J. Inorg. Chem.*(无机化学学报), **2012**,**28**(5):983-988

[34]Chen H, Hu Q, Peng W, et al. *Ceram. Int.*, **2017**,**43**(14): 10919-10926

[35]Li N, He Y, Wang X, et al. *Electrochim. Acta*, **2017**,**231**: 363-370